J|A|C|S ARTICLES

Published on Web 10/06/2010

Stability and Reactivity of $\epsilon-\chi-\theta$ Iron Carbide Catalyst Phases in Fischer−Tropsch Synthesis: Controlling μ_C

Emiel de Smit,[†] Fabrizio Cinquini,[‡] Andrew M. Beale,[†] Olga V. Safonova,[§] Wouter van Beek,[§,||] Philippe Sautet,*[,‡] and Bert M. Weckhuysen*[,†]

Inorganic Chemistry and Catalysis, Debye Institute for Nanomaterials Science, Utrecht University, Sorbonnelaan 16, 3584 CA Utrecht, The Netherlands, Université de Lyon, Institut de Chimie de Lyon, Laboratoire de Chimie, École Normale Supérieure de Lyon and CNRS, 46 Allée d'Italie, F-69364 Lyon Cedex 07, France, Swiss-Norwegian Beamlines, European Synchrotron Radiation Facility, 6 Rue Jules Horowitz, BP220, F-38043 Grenoble Cedex, France, and Dipartimento di Scienze e Tecnologie Avanzate and Nano-SiSTeMI Interdisciplinary Centre, Università del Piemonte Orientale 'A. Avogadro', Viale T. Michel 11, 15121 Alessandria, Italy

Received July 2, 2010; E-mail: philippe.sautet@ens-lyon.fr; b.m.weckhuysen@uu.nl

Abstract: The stability and reactivity of ϵ, χ, and θ iron carbide phases in Fischer−Tropsch synthesis (FTS) catalysts as a function of relevant reaction conditions was investigated by a synergistic combination of experimental and theoretical methods. Combined *in situ* X-ray Absorption Fine Structure Spectroscopy/X-ray Diffraction/Raman Spectroscopy was applied to study Fe-based catalysts during pretreatment and, for the first time, at relevant high pressure Fischer−Tropsch synthesis conditions, while Density Functional Theory calculations formed a fundamental basis for understanding the influence of pretreatment and FTS conditions on the formation of bulk iron carbide phases. By combining theory and experiment, it was found that the formation of θ-Fe_3C, χ-Fe_5C_2, and ϵ-carbides can be explained by their relative thermodynamic stability as imposed by gas phase composition and temperature. Furthermore, it was shown that a significant part of the Fe phases was present as amorphous carbide phases during high pressure FTS, sometimes in an equivalent amount to the crystalline iron carbide fraction. A catalyst containing mainly crystalline χ-Fe_5C_2 was highly susceptible to oxidation during FTS conditions, while a catalyst containing θ-Fe_3C and amorphous carbide phases showed a lower activity and selectivity, mainly due to the buildup of carbonaceous deposits on the catalyst surface, suggesting that amorphous phases and the resulting textural properties play an important role in determining final catalyst performance. The findings further uncovered the thermodynamic and kinetic factors inducing the $\epsilon-\chi-\theta$ carbide transformation as a function of the carbon chemical potential μ_C.

1. Introduction

Fischer−Tropsch synthesis (FTS) converts synthesis gas (CO and H_2) into longer straight chain hydrocarbons by a surface polymerization reaction,[1] making it an important pathway to produce valuable chemicals and transportation fuels from carbon sources alternative to crude oil (e.g., natural gas, coal, and biomass). Most group VIII transition metals are active in the reaction, but only Fe and Co are typically applied industrially, owing to their high selectivity to long hydrocarbon chains and economic feasibility of the overall FTS process. Fe-based catalysts, in particular, have gained interest recently[2] due to the low costs and high availability of the metal, a tunable product distribution (e.g., toward olefins and alcohols), and the prospects of converting coal or biomass-borne synthesis gas[3] which typically have low H_2/CO ratios with respect to the needed stoichiometric ratio for FTS of 2. The latter benefit is due to the fact that, unlike Co-based catalysts, Fe-based catalysts (more specifically Fe_3O_4) also catalyze the water−gas shift (WGS) reaction:

$$CO + H_2O \leftrightarrow CO_2 + H_2 \quad (1)$$

which effectively increases the H_2/CO ratio during FTS.

The Fe-based FTS catalyst shows a rich phase chemistry under pretreatment and FTS conditions, making it a challenging system to study.[4] Depending on the pretreatment method, Fe-based FTS catalyst precursors undergo several phase transitions before becoming active in the FTS reaction. Typically, iron oxide based precursors are activated in a reduction treatment in H_2, CO, or mixtures thereof, and depending on the conditions used, metallic Fe or iron carbides are formed.[5−7] Both metallic Fe and iron carbide surfaces can dissociate and hydrogenate

[†] Utrecht University.
[‡] École Normale Supérieure de Lyon and CNRS.
[§] European Synchrotron Radiation Facility.
[||] Università del Piemonte Orientale 'A. Avogadro'.

(1) Anderson, R. B., *The Fischer−Tropsch Synthesis*. Academic Press: New York, 1984.
(2) de Smit, E.; Weckhuysen, B. M. *Chem. Soc. Rev.* **2008**, *37*, 2758–2781.
(3) van Steen, E.; Claeys, M. *Chem. Eng. Technol.* **2008**, *31*, 655–666.
(4) de Smit, E.; Swart, I.; Creemer, J. F.; Hoveling, G. H.; Gilles, M. K.; Tyliszczak, T.; Kooyman, P. J.; Zandbergen, H. W.; Morin, C.; Weckhuysen, B. M.; de Groot, F. M. F. *Nature* **2008**, *456*, 222–225.
(5) de Smit, E.; Beale, A. M.; Nikitenko, S.; Weckhuysen, B. M. *J. Catal.* **2009**, *262*, 244–256.

 10.1021/ja105853q

CO,[8,9] but under FTS conditions carbides readily form due to the proposed similarity between activation barriers of carbon diffusion into the metallic Fe body centered cubic (bcc) structure and hydrogenation and polymerization at the surface.[10]

During FTS ϵ-Fe_2C, ϵ'-$Fe_{2.2}C$, Fe_7C_3, χ-Fe_5C_2, and θ-Fe_3C have all been observed;[6,11−13] nevertheless, the exact role of each carbide phase in the catalytic reaction remains unclear.[2] While research efforts have been committed to comparing the activity and stability of formed phases during FTS[14−17] these studies have been hindered by the small crystallite sizes involved and by the fact that Fe-based catalysts are easily oxidized upon exposure to air, making correct *ex situ* characterization difficult and advocating the need for *in situ* characterization of the catalysts,[4,5,18,19] where possible under realistic reaction conditions (i.e., *operando*). As a result, there is an ongoing debate on the exact nature of the active phase and site in Fe-based FTS catalysts. In a previous study,[5] we reported on the *in situ* characterization of H_2 and CO/H_2 pretreated, promoted, and unpromoted Fe-based catalysts during FTS at 1 bar and illustrated the complexity of the different carbide phases that are formed on a local and long-range order scale. Industrially, however, FTS is performed at elevated pressures (typically ∼20 bar) and to our best knowledge, unlike Co-based catalysts,[20−22] Fe-based catalysts have not yet been characterized *in situ* under high pressure FTS conditions.

Iron carbides are best classified as interstitial carbides.[23] Carbon atoms are placed in available interstitial sites in a distorted hexagonally closed packed (hcp) structure of (zerovalent) Fe atoms. The structure of iron carbides can be classified, according to the site occupation of the carbon atoms in the crystal structure, into trigonal prismatic (TP) carbides and octahedral carbides (O).[24] In the context of metallurgy, the transformation of iron carbides has been studied intensively. At low temperature a transition of O carbides to TP carbides is observed. More specifically, ϵ-carbides, formed by martensitic shearing,[25] are observed to form up to ∼250 °C. The ϵ-carbides transform into χ-Fe_5C_2 above 250 °C and subsequently to θ-Fe_3C above 350 °C by twinning.[26,27] The exact temperature of transformation is dependent on many factors, such as crystallite sizes, morphology and surface texture, and the presence of promotors or inhibitors for the formation of specific carbide phases (such as Si and Al).

In catalysis, understanding of the influence of experimental reaction conditions on the carbide phase chemistry is relatively limited. Therefore, in this paper we will investigate the thermodynamics of the (trans)formation of bulk carbide phases during catalyst pretreatment and the subsequent influence of the formed phases on the performance during FTS at relevant high pressure conditions by a combination of theoretical and experimental methods. An ab initio atomistic thermodynamics approach is applied to predict the relative stability of bulk carbide phases by discussing the influence of the carbon chemical potential μ_C imposed by the reservoir of gas phase species. In parallel, combined *in situ* X-ray Diffraction (XRD)/X-ray Absorption Fine Structure Spectroscopy (XAFS)/Raman Spectroscopy is applied to study Fe phases and associated carbonaceous species in Fe-based catalysts during pretreatment and FTS under relevant high pressure conditions. The combination of XRD and XAFS allows for the detailed study of bulk inorganic crystalline and amorphous phases present in the materials under study, while Raman allows the acquisition of complementary information about the organic carbonaceous surface species formed. This integrated theoretical/experimental approach will enable us to examine the $\epsilon-\chi-\theta$ transition from a novel viewpoint, obtain valuable structure−FTS performance correlations, and show how different carbide phases may be synthesized during catalyst pretreatment by controlling μ_C.

2. Experimental Methods

2.1. Computational Details. Spin-Polarized Density Functional Theory (DFT) calculations were performed in the generalized gradient approximation (GGA) using the Perdew−Wang (PW91)[28] functional as implemented in the VASP[29,30] code. The projected augmented wave (PAW) method has been adopted. The energy cutoff for the plane wave basis set was set to 400 eV, in accordance with the selected PAW atomic radii. The convergence of the total energy was confirmed for different *k*-point meshes and cutoff energies.

Ab initio atomistic thermodynamics was applied to compare the relative stability of carbide phases under different relevant catalytic and pretreatment conditions. In our approach, the absorption energy of carbon in bulk carbides is calculated from DFT total energy calculations, as a function of the carbon chemical potential μ_C, using bcc α-Fe as a reference:

(6) Bukur, D. B.; Okabe, K.; Rosynek, M. P.; Li, C. P.; Wang, D. J.; Rao, K.; Huffman, G. P. *J. Catal.* **1995**, *155*, 353–365.
(7) Sudsakorn, K.; Goodwin, J. G.; Adeyiga, A. A. *J. Catal.* **2003**, *213*, 204–210.
(8) Petersen, M. A.; van den Berg, J.-A.; van Rensburg, W. J. *J. Phys. Chem. C* **2010**, *114*, 7863–7879.
(9) Gracia, J.; Prinsloo, F.; Niemantsverdriet, J. *Catal. Lett.* **2009**, *133*, 257–261.
(10) Niemantsverdriet, J. W.; van der Kraan, A. M. *J. Catal.* **1981**, *72*, 385–388.
(11) Niemantsverdriet, J. W.; van der Kraan, A. M.; van Dijk, W. L.; van der Baan, H. S. *J. Phys. Chem.* **1980**, *84*, 3363–3370.
(12) Raupp, G. B.; Delgass, W. N. *J. Catal.* **1979**, *58*, 337–347.
(13) Datye, A. K.; Jin, Y.; Mansker, L.; Motjope, R. T.; Dlamini, T. H.; Coville, N. J., The nature of the active phase in iron Fischer−Tropsch catalysts. In *Stud. Surf. Sci. Catal.*, Elsevier: 2000; Vol. 130, pp 1139−1144.
(14) Pijolat, M.; Perrichon, V.; Bussière, P. *J. Catal.* **1987**, *107*, 82–91.
(15) Herranz, T.; Rojas, S.; Pérez-Alonso, F. J.; Ojeda, M.; Terreros, P.; Fierro, J. L. G. *J. Catal.* **2006**, *243*, 199–211.
(16) Bukur, D. B.; Lang, X.; Ding, Y. *Appl. Catal. A-Gen.* **1999**, *186*, 255–275.
(17) Jung, H.; Thomson, W. J. *J. Catal.* **1992**, *134*, 654–667.
(18) Janbroers, S.; Louwen, J. N.; Zandbergen, H. W.; Kooyman, P. J. *J. Catal.* **2009**, *268*, 235–242.
(19) Ribeiro, M. C.; Jacobs, G.; Davis, B. H.; Cronauer, D. C.; Kropf, A. J.; Marshall, C. L. *J. Phys. Chem. C* **2010**, *114*, 7895–7903.
(20) Bezemer, G. L.; Remans, T. J.; van Bavel, A. P.; Dugulan, A. I. *J. Am. Chem. Soc.* **2010**, *132*, 8540–8541.
(21) Rønning, M.; Tsakoumis, N. E.; Voronov, A.; Johnsen, R. E.; Norby, P.; van Beek, W.; Borg, Ø.; Rytter, E.; Holmen, A., *Catal. Today In Press, Corrected Proof, doi: http://dx.doi.org/10.1016/j.cattod.2009.10.010*.
(22) Karaca, H.; Hong, J.; Fongarland, P.; Roussel, P.; Griboval-Constant, A.; Lacroix, M.; Hortmann, K.; Safonova, O. V.; Khodakov, A. Y. *Chem. Commun.* **2010**, *46*, 788–790.
(23) Toth, L. E., *Transition Metal Carbides and Nitrides*. Academic Press: New York, 1971.
(24) Le Caër, G.; Dubois, J. M.; Pijolat, M.; Perrichon, V.; Bussière, P. *J. Phys. Chem.* **1982**, *86*, 4799–4808.
(25) Jack, K. H. *J. Iron Steel Inst. London* **1951**, *169*, 26–36.
(26) Andersson, S.; Hyde, B. G. *J. Solid State Chem.* **1974**, *9*, 92–101.
(27) Nagakura, S. *J. Phys. Soc. Jpn.* **1959**, *14*, 186–195.
(28) Perdew, J. P.; Chevary, J. A.; Vosko, S. H.; Jackson, K. A.; Pederson, M. R.; Singh, D. J.; Fiolhais, C. *Phys. Rev. B* **1992**, *46*, 6671–6687.
(29) Kresse, G.; Hafner, J. *Phys. Rev. B* **1993**, *47*, 558–561.
(30) Kresse, G.; Furthmüller, J. *Phys. Rev. B* **1996**, *54*, 11169–11186.

$$E_{abs} = \frac{E_{totalFe_xC_y} - x \cdot E_{totalFe_{bcc}} - y \cdot \mu_C}{y} \quad (1a)$$

The carbon chemical potential μ_C is imposed by the surrounding gas mixture at a certain temperature and pressure. For instance, for the reaction

$$2CO \rightarrow CO_2 + C \quad (2)$$

$$\mu_C = 2\mu_{CO} - \mu_{CO_2} \quad (3)$$

The chemical potential μ_C of each species can be calculated by statistical thermodynamics (details provided in the Supporting Information). Gas phase molecules were optimized and the total energy and the vibrational frequencies were determined using VASP, while the rotational and translational partition functions were evaluated using GAUSSIAN 03.[31]

The interaction energy between C and Fe atoms in the different Fe_xC_y carbide structures can be determined by using atomic carbon as a reference, from

$$E_{int} = \frac{E_{totalFe_xC_y} - E_{totalref} - y \cdot \mu_{Cref}}{y} \quad (4)$$

while the deformation energies, normalized per carbon atom, can be calculated using

$$E_{def} = E_{abs} - E_{int} = \frac{E_{totalref} - x \cdot E_{totalFe_{bcc}}}{y} \quad (5)$$

where $E_{totalref}$ is the total energy of the carbide structure without any C atoms. Note that we have used the bcc α-Fe atom as a reference here, even though the iron carbide structures are derived from an hcp lattice. As a result, the deformation energies calculated here also contain a (constant) energy contribution for the rearrangement of the bcc to the hcp lattice. The deformation energy can be used to express the amount of deformation of the structure from the ideal Fe bcc structure and is used as a qualitative indication for the amount of strain in the carbide structure.

Table 1 lists the characteristics of the carbide crystal structures used as the initial input structure for the DFT calculations. Figure S1 in the Supporting Information gives a visual overview of the crystal structure unit cells. In this paper we only report on the carbide phases that have been observed experimentally or are predicted to be stable during FTS. Other structures (e.g., Fe_4C) have been tested, but they were found to be thermodynamically unstable under typical FTS conditions and, hence, will not be further discussed.

After the initial structure optimization, the theoretical X-ray diffraction (XRD) patterns of the calculated crystal structures were determined and compared with experimental XRD patterns. It was found that in some DFT optimizations the carbide structure would be modified toward a structure with a lower total energy per unit volume, but with an unrealistic (not reported) crystal structure and XRD pattern. Since the TP carbide phases can be built from twinning operations on the same parent hcp structure as O carbides,[26] during the structure optimization the initial carbide structures might be transformed into a different, enthalpically more stable carbide structure. As the DFT optimizations do not take into account the entropic contribution to the total free energy of the crystal structures, this has been observed for crystal structures that are stabilized at higher temperatures by a contribution in vibrational entropy, for example ZrO_2.[32,33] Because the entropic contribution is not included in our DFT calculations, in order to prevent reporting structurally incorrect carbide structures and associated energies, the simulated XRD patterns were taken as a criterion for the correctness calculations and, where needed, a constraint was applied on the shape of the unit cell.

Fe atoms have a higher X-ray scattering cross section in comparison to (low Z) C atoms in the crystal structures. As a result, there is a certain level of uncertainty to the position of carbon atoms in the crystal structures as determined by XRD. We found that the position of carbon atoms inside the unit cells did not significantly change the calculated XRD patterns (Figure S2 in the Supporting Information). Because of this, and in order to obtain reliable DFT results, we allowed all Fe and C atoms to fully relax inside the unit cells. The applied XRD criterion (Figure S2) and some special considerations on the structure model of the carbides under study are summarized in the Supporting Information.

2.2. Materials. A high surface area α-Fe_2O_3 catalyst was synthesized by precipitation from a 0.6 M $Fe(NO_3)_3 \cdot 9H_2O$ (Acros, 98+ %) solution using a Na_2CO_3 (Acros, anhydrous, pure) solution (2.0 M) as a precipitation agent. The $Fe(NO_3)_3$ solution was heated to ~90 °C and added (in ~1 min) to the near boiling Na_2CO_3 solution under vigorous stirring. The resulting precipitate was separated by filtration and reslurried and washed four times in 1 L of hot (~90 °C) distilled water until all residual sodium was removed. The precipitate was dried in stagnant air for 6 h at 60 °C and 24 h at 120 °C. Finally, the dried catalyst precursor was crushed, sieved to a 200−500 μm particle size, and calcined in high air flow at 300 °C for 5 h using a heating ramp of 5 °C/min.

For reference experiments, a commercial high purity α-Fe_2O_3 reference (Sigma Aldrich, 99.999%) was obtained.

The purity of the catalyst material and α-Fe_2O_3 reference was confirmed by X-ray Fluorescence (XRF) analysis on a Goffin Meyvis Spectro X-lab 2000 machine.

2.3. Ex Situ Experiments. α-Fe_2O_3 catalysts samples were pretreated in different mixtures of CO/H_2 (CO, 99.0%, Linde; H_2, 99.9%, Linde). For each experiment, about 100 mg of the powdered samples were diluted in ~500 mg of SiC and loaded into a tubular glass reactor with an internal diameter of 0.5 cm. The reactor was heated in a tubular quartz oven while thermocouples monitored the temperature of the sample bed. The samples were treated in 20 mL/min flow CO/H_2 mixtures or pure H_2 and heated at 2 °C/min up to the desired temperature and kept at this temperature for 2 h.

The iron carbide reference and catalyst materials were characterized *ex situ* using N_2 physisorption, Transmission Electron Microscopy (TEM), and X-ray Powder Diffraction (XRD).

The Brunauer−Emmett−Teller (BET) surface area and total pore volume of the catalyst materials were determined from N_2-physisorption. N_2-physisorption isotherms were measured at −196 °C using a Micromeritics Tristar 3000 apparatus. The samples were dried in a He flow for 14 h at 200 °C (5 °C/min ramp) prior to analysis.

TEM images were acquired using a Tecnai 20F FEG microscope operating at 200 kV and equipped with Energy Dispersive X-ray (EDX) and Selected Area Diffraction (SAD) analyzers, allowing obtaining information about the crystallinity and distribution of chemical species on the catalysts.

XRD powder diffraction patterns were acquired on a Bruker D8 X-ray powder diffractometer equipped with a Co Kα X-ray tube ($\lambda = 1.7902$ Å). For comparison with the *in situ* experiments, the angles of the diffraction peaks were converted to 2θ values corresponding to $\lambda = 0.5$ Å.

2.4. In Situ Experiments. X-ray Absorption Fine Structure (XAFS), X-ray Powder Diffraction (XRD), and Raman Spectroscopy data were collected on the Swiss Norwegian Beamlines bending magnet station BM1B (SNBL, BM1B) at the European Synchrotron Radiation Facility (ESRF) in Grenoble, France. The storage ring operated at 6 GeV and 200 mA in 7/8 + 1 multibunch

(31) Frisch, M. J.; et al. *Gaussian 03*, Revision C.02; Gaussian, Inc.: Wallingford, CT, 2003.

(32) Sternik, M.; Parlinski, K. *J. Chem. Phys.* **2005**, *123*, 1–6.

(33) Orlando, R.; Pisani, C.; Ruiz, E.; Sautet, P. *Surf. Sci.* **1992**, *275*, 482–492.

Table 1. Summary of the Crystal Structures Used As Input for the DFT Structure Optimizations

Iron Carbide	Space Group	Lattice parameters (Å)	Angles	Carbon Concentration (C atoms Å^{-3})
ϵ-Fe_3C[58]	$P6_322$ (182)	$a = b = 4.767$, $c = 4.354$	$\alpha = \beta = 90°$, $\gamma = 120°$	0.0233
θ-Fe_3C[59]	*Pnma* (62)	$a = 5.092$, $b = 6.741$, $c = 4.527$	$\alpha = \beta = \gamma = 90°$	0.0257
ϵ'-$Fe_{2.2}C$[38,60 a]	$P6_3/mmc$ (194)	$a = b = 2.749$, $c = 4.340$	$\alpha = \beta = 90°$, $\gamma = 120°$	0.0298
χ-Fe_5C_2[61]	$C2/c$ (15)	$a = 11.588$, $b = 4.579$, $c = 5.059$	$\alpha = \gamma = 90°$, $\beta = 97.746$	0.0301
Fe_7C_3[62]	$P6_3mc$ (186)	$a = b = 6.882$, $c = 4.54$	$\alpha = \beta = 90°$, $\gamma = 120°$	0.0322
ϵ-Fe_2C[38,60 a]	$P6_3/mmc$ (194)	$a = b = 2.749$, $c = 4.340$	$\alpha = \beta = 90°$, $\gamma = 120°$	0.0340
η-Fe_2C[63]	*Pnnm* (58)	$a = 4.704$, $b = 4.318$, $c = 2.830$	$\alpha = \beta = \gamma = 90°$	0.0348

[a] A supercell of $2 \times 2 \times 2$ unit cells was used for the calculations.

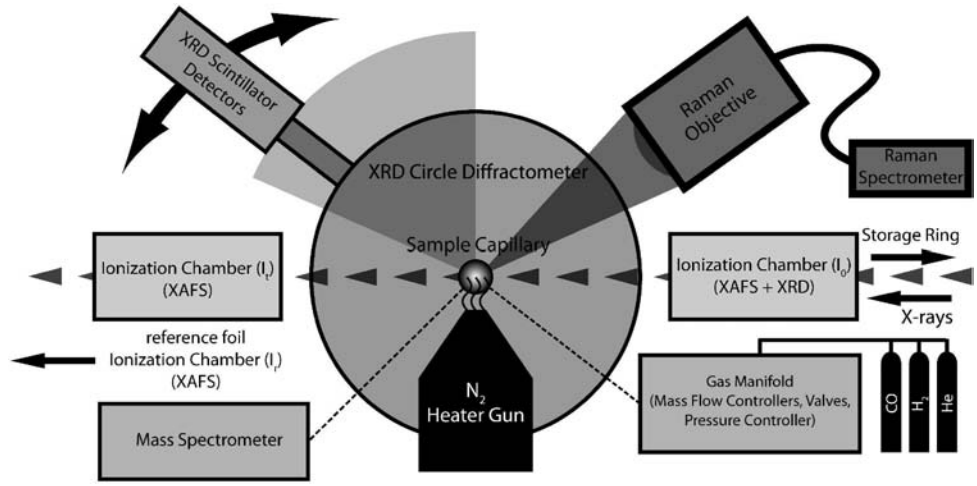

Figure 1. Schematic representation of the Combined XAFS/XRD/Raman experimental setup.

filling mode. A schematic representation of the setup is shown in Figure 1. A more detailed description of the setup is given in the Supporting Information.

2.5. Carbide References. χ-Fe_5C_2 and θ-Fe_3C carbide reference materials were synthesized and characterized *in situ* by exposing the α-Fe_2O_3 reference material to a flow of 10 mL/min CO (99.0%, Linde) and heating it up to the desired temperature at 2 °C/min. χ-Fe_5C_2 was synthesized by dwelling 2 h at 350 °C for 2 h. θ-Fe_3C was synthesized by dwelling at 450 °C for 2 h. More details about the preparation and characterization of the carbide references are given in the Supporting Information Figures S4−S8 and Table S1.

2.6. In Situ High Pressure FTS. The α-Fe_2O_3 catalyst samples were converted into different carbide phases and characterized *in situ* using the XAFS/XRD/Raman techniques. The first sample was pretreated by heating the catalyst precursor in CO (5 mL/min, 99.0%, Linde) to 280 °C (2 °C/min) for 2 h. This pretreatment is referred to as the high μ_C pretreatment. The second sample was pretreated by heating the catalyst precursor in a 1% CO/H_2 mixture (10 mL/min, (H_2, 99.99%, Linde)) to 350 °C for 2 h (2 °C/min ramp). This pretreatment will be referred to as the low μ_C pretreatment.

After activation, the catalysts were cooled to 250 °C and exposed to CO/H_2 gas (5:5 mL/min). Subsequently, the pressure was slowly increased to 10 bar over a period of 2 h. The samples were run at 10 bar for 6 h. It is noted here that a recent study suggested that the capillary reactor exhibits quasi plug flow conditions.[34] Catalytic reaction data during the experiment were measured using an online mass spectrometer connected to the capillary reactor outlet. The reported mass spectrometry data are normalized per g of Fe.

2.7. Data Analysis. Crystal domain sizes and volume fractions of the crystalline phases in the samples were estimated by refining the diffraction profiles and estimating the line broadening using the POWDERCELL software package,[35] while taking into account the differences in experimental broadening between the used synchrotron and laboratory setups. Peak shapes were fitted using Pseudo-Voigt profiles. Figure S3 in Supporting Information shows a typical example of a refined experimental XRD pattern. Fe K-edge Extended X-ray Absorption Fine Structure (EXAFS) data analysis was carried out using the XDAP software package.[36] The analysis procedures are summarized in the Supporting Information. Fe K-edge XANES analysis and linear combination fitting were carried out within the ATHENA[37] program, which is based on the IFEFFIT library of numerical and XAS algorithms. For calculation of the carbide X-ray Absorption Near Edge Structure (XANES) spectra, the real space full multiple scattering FEFF code was used. Details about the calculations are summarized in the Supporting Information.

3. Results and Discussion

3.1. Ab Initio Atomistic Thermodynamics Calculations. Figure 2 shows a plot of the volume normalized absorption energy (Ω) of the different carbide phases as a function of the chemical potential μ_C, as well as the μ_C values imposed by different, relevant gas mixtures applied in the pretreatment of Fe-based catalysts and the FTS reaction. At a higher carbon chemical potential, the carbide phases are more stable than the pure bcc α-Fe metal (E_{ads} and $\Omega < 0$). The critical value μ_C^{crit}, for which the absorption energy E_{ads} becomes negative and carbides become stable with respect to free carbon and bcc α-Fe, is given in Table 2. From the table, it is clear that μ_C^{crit} is similar for all

(34) Grunwaldt, J. D.; Caravati, M.; Hannemann, S.; Baiker, A. *Phys. Chem. Chem. Phys.* **2004**, *6*, 3037–3047.
(35) Kraus, W.; Nolze, G. *J. Appl. Crystallogr.* **1996**, *29*, 301–303.
(36) Vaarkamp, M.; Linders, J. C.; Koningsberger, D. C. *Physica B: Condensed Matter* **1995**, *208−209*, 159–160.
(37) Ravel, B.; Newville, M. *J. Synchrotron Radiat.* **2005**, *12*, 537–541.
(38) Dirand, M.; Afqir, L. *Acta Metall.* **1983**, *31*, 1089–1107.

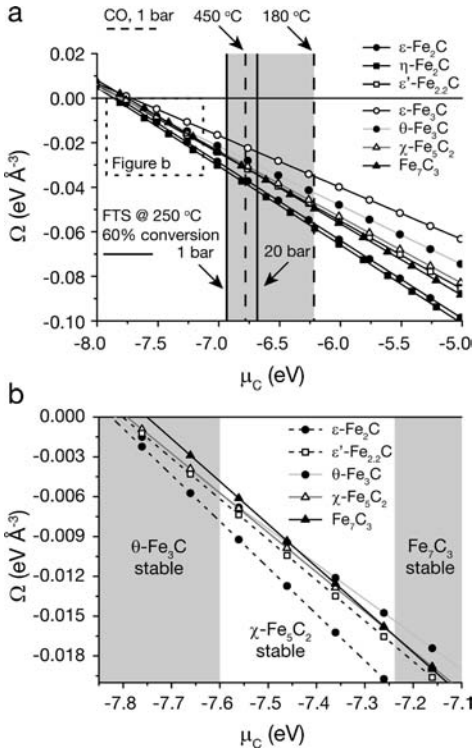

Figure 2. Volume normalized absorption energy (Ω) of iron carbide phases as a function of μ_C. (a) The shaded area represents the experimental range of μ_C applied in this study. Vertical lines indicate the specific μ_C imposed by several gas phase mixtures (pCO/pCO$_2$ = 2:1 for CO at 1 bar and pCO/pH$_2$/pH$_2$O = 2:3:5 for FTS at 60% conversion). (b) detail of the graph in (a), emphasizing the stability ranges of TP carbide phases.

Table 2. Selected Bulk Iron Carbide Structural Parameters from DFT Structure Optimization

Iron Carbide	μ_C^{crit} (eV C atom^{-1})	Interaction energy (eV C atom^{-1})	Deformation Energy (10^{-2} eV C atom^{-1})	Carbon Concentration (C atoms Å^{-3})
η-Fe$_2$C	−7.864	−9.485	1.62	0.0353
ϵ-Fe$_2$C	−7.825	−9.526	1.70	0.0350
θ-Fe$_3$C	−7.818	−9.170	1.35	0.0265
ϵ'-Fe$_{2.2}$C	−7.796	−9.736	1.94	0.0306
χ-Fe$_5$C$_2$	−7.792	−8.632	0.84	0.0298
Fe$_7$C$_3$	−7.751	−8.849	1.10	0.0322
ϵ-Fe$_3$C	−7.719	−10.238	2.52	0.0233

carbide phases under study. This can be rationalized by the structural similarity of the carbide phases. Carbon atoms in the η-Fe$_2$C structure have the lowest μ_C^{crit}. The order at which the carbides become stable with respect to "free" C and bcc α-Fe upon increasing μ_C, when not taking into account any other effects, can be inferred from Table 2 and is η-Fe$_2$C > ϵ-Fe$_2$C > θ-Fe$_3$C > ϵ'-Fe$_{2.2}$C > χ-Fe$_5$C$_2$ > Fe$_7$C$_3$ > ϵ-Fe$_3$C. However, the formation of carbide phases is likely to be dependent not only on the kinetics of formation[25,26,38] and but also on thermodynamics. Furthermore, the C absorption energies in the structures are close (all structures within ∼0.1 eV/C atom), but the concentration of C in each structure is different. Therefore, the stability of the carbide structures is highly dependent on the μ_C imposed by the chemical (gas phase) surroundings, as seen in Figure 2.

Figure 3 summarizes some general implications of reaction conditions on the chemical potential μ_C. Overall, it follows that higher temperatures and lower CO partial pressures yield a lower μ_C. It can also be inferred from the figure that, at the pressure

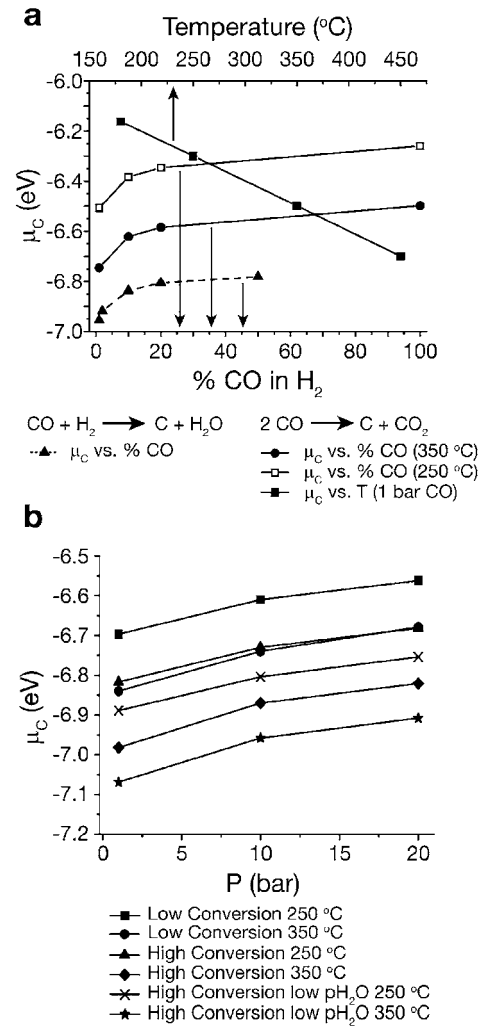

Figure 3. Influence of the gas phase conditions on μ_C. (a) μ_C as a function of mixtures of CO in H$_2$ at 1 bar at 250 or 350 °C, for the reaction 2 CO → CO$_2$ + C, plotted together with the temperature dependence of μ_C in for the same reaction in 1 bar CO (pCO/pCO$_2$) = 2:1. Also included is μ_C for the reaction CO + H$_2$ → C + H$_2$O for same gas mixtures (pH$_2$O = 0.01 bar). (b) μ_C as a function of different FTS conditions. High conversion = 60%, pCO/pH$_2$/pH$_2$O = 2:3:5. For low H$_2$O, pCO/pH$_2$/pH$_2$O = 2:3:1. Low conversion = 5%, pCO/pH$_2$/pH$_2$O = 100:100:5.

conditions considered here, the dependence of μ_C is typically more sensitive to temperature than to pressure. It is noted, however, that the H$_2$O partial pressure can also have a great influence on μ_C.

The basic result here is that, under FTS conditions, the carbon chemical potential is such that Fe carbide structures are clearly more stable than metallic Fe. The relative stability of the various carbide structures is more subtle and will be discussed in more detail below.

From Figure 2, it can be seen that the volume based absorption energy as a function of μ_C is lowest for the η-Fe$_2$C and ϵ-Fe$_2$C and ϵ'-Fe$_{2.2}$C carbides, which means that these structures are most stable for the entire carbide stability domain. This would mean that none of the TP carbides (θ-Fe$_3$C, χ-Fe$_5$C$_2$, and Fe$_7$C$_3$) are stable with respect to the O carbides over the entire range of μ_C. However, TP carbides are commonly observed experimentally. In fact, η-Fe$_2$C has only been reported to form during high temperature steel tempering[38] and not under typical FTS and catalyst pretreatment conditions. Furthermore, ϵ-Fe$_2$C and ϵ'-Fe$_{2.2}$C are usually not the major carbide phases

observed during FTS.[12,24,39] As the calculations presented in Figure 2 do not include entropic and kinetic considerations, it is postulated that the formation of O carbide phases is entropically and kinetically unfavored. In support of this, it is well-known that ϵ-carbides typically form under low temperature conditions (<200 °C). This is in good agreement with their calculated energetic stability, since at lower temperatures the entropic contribution to the free energy is small and therefore it is dominated by the internal energy contribution. At higher temperature pretreatment and FTS conditions, however, the entropy term might become more important, and it is postulated here that this plays an important role in the relative stability of the carbide phases. Finally, the fact that TP carbide structures (most notably χ-Fe_5C_2) transformed into other carbide structures during the structure optimizations might be an indicator for significant entropic contributions to the free energy of these structures.[32,33]

Kinetically, the formation of O carbide phases might also be hindered. Table 2 shows the interaction energy between C and Fe atoms in the different carbide structures and their deformation energy with respect to an Fe bcc lattice. From the table, it can be seen that the deformation energy is most significant in the case of the η-Fe_2C and ϵ-carbide structures. The TP carbide structures typically observed during FTS, θ-Fe_3C, χ-Fe_5C_2, and Fe_7C_3, share low deformation energies. In addition to the high deformation energy, the stoichiometrically needed amount of carbon in the ϵ-Fe_2C and η-Fe_2C structures may be limited by the diffusion of carbon into the bcc α-Fe lattice, as further supported by the typical experimentally observed ϵ-$Fe_{2.2}C$ stoichiometry. As the hcp lattice of Fe atoms is formed, twinning becomes a feasible way to release strain and adopt a TP structure with lower deformation energy and higher entropy. It is therefore proposed that the O carbides, although having a lower internal energy contribution, are transformed into the χ-Fe_5C_2 phase at higher temperature due to the combination of lower strain, carbon diffusion limitations, and a lower vibrational entropy, ultimately resulting in a higher relative thermodynamic stability and kinetic preference for χ-Fe_5C_2 at lower μ_C. In support of this, ϵ-Fe_2C and ϵ'-$Fe_{2.2}C$ are commonly reported after carburization low temperatures (high μ_C), for small particles sizes (less diffusion limitations) and in the presence of a support material or chemical promoters.[6,11] Under these conditions, the formation of the ϵ-carbide phases might be preferred.

The ϵ-Fe_3C phase, apart from being thermodynamically unstable with respect to χ-Fe_5C_2, has an especially high deformation energy and therefore is not likely to form under typical FTS (pretreatment) conditions. It is further postulated that the orthorhombic η-Fe_2C phase does not form under typical catalytically relevant conditions because of the lower configurational entropy as a result of the ordered placement of carbon atoms in this structure with respect to the more disordered ϵ-carbides. In the remainder of the paper we will not further discuss the possible formation of the η-Fe_2C phase and focus the discussion on the O and TP carbide phases that have been reported under FTS conditions.

Figure 2b illustrates the effect of μ_C on the stability of the TP χ-Fe_5C_2, θ-Fe_3C, and Fe_7C_3 phases. From the figure it is clear that the χ-Fe_5C_2 and θ-Fe_3C phases become relatively more stable with respect to the ϵ-carbides at lower μ_C (higher temperature, lower CO pressure). However, as discussed above, in absolute (enthalpic) terms ϵ'-$Fe_{2.2}C$ and ϵ-Fe_2C are still predicted to be the more stable than χ-Fe_5C_2 for every μ_C. It can be inferred from the figure that only at very low μ_C (−7.7 eV) the θ-Fe_3C phase is more stable than ϵ'-$Fe_{2.2}C$.

θ-Fe_3C becomes stable with respect to χ-Fe_5C_2 at low μ_C (−7.6 eV) conditions. This explains why, in pure CO, θ-Fe_3C is only formed from χ-Fe_5C_2 at higher temperature (>350 °C).[27] In addition the carbon concentration of the carbide structure changes significantly in this transformation, and it is likely that carbon diffusion plays a major role in the kinetic formation of this phase.[40]

Figure 2b further shows that Fe_7C_3 is stable with respect to χ-Fe_5C_2 at higher μ_C (~7.25 eV). At low temperatures (imposing high μ_C conditions) however, it is expected that there is significant (kinetic) competition between the formation of the Fe_7C_3 phase and ϵ-carbides. This might mean that the Fe_7C_3 phase is difficult to form experimentally since at low temperature there is competition with the ϵ-carbide phases and at higher temperature (low μ_C) conditions χ-Fe_5C_2 and θ-Fe_3C are more stable. It has been proposed that Fe_7C_3 can be constructed from a twinning operation on the θ-Fe_3C structure.[41] Therefore, we suggest that this carbide may form from θ-Fe_3C under extreme experimental conditions,[42] i.e. at high μ_C in combination with high temperatures. It is noted that the Fe_7C_3 carbide is most commonly reported in high pressure, high temperature Fischer−Tropsch synthesis and commercial reactors after long reaction times,[13] where the high pressure makes μ_C more favorable for the formation of this phase and the high temperature and long reaction times favor the kinetics of formation.

Our calculations do not take into account kinetic factors. Therefore, the reversibility of the carbide transformations cannot be accurately predicted. Experimentally, it is typically observed that the formation of carbide phases from α-Fe is more rapid than the interconversion of carbide phases. Diffusion of carbon in the carbide structures is likely to play an important role. However, in pure H_2 at higher temperatures, constituting extremely low μ_C conditions in combination with favorable kinetic conditions, carbide phases can be readily transformed back into α-Fe.

Taking into account the discussion above, our calculations qualitatively describe the $\epsilon-\chi-\theta$ transformation reported for iron carbides. Scheme 1 summarizes the predicted formation of the different carbide phases as a function of μ_C.

Ab initio thermodynamic calculations have been successfully applied to many catalytic problems.[43−45] However, in Figure 2, there is an offset between the calculated μ_C as imposed by the gas phase and the stability regions of the carbides. For example, θ-Fe_3C is known to form in CO atmospheres above 350 °C,[27] while from Figure 2b it follows that the phase is not stable at the calculated μ_C of −6.7 eV ($pCO/pCO_2 = 2:1$, $p_{total} = 1.0$ bar, $T = 350$ °C) but only becomes stable with respect to χ-Fe_5C_2 at −7.6 eV. This could be due to several reasons.

(39) Amelse, J. A.; Butt, J. B.; Schwartz, J. H. *J. Phys. Chem.* **1978**, *82*, 558–563.
(40) Königer, A.; Hammerl, C.; Zeitler, M.; Rauschenbach, B. *Phys. Rev. B* **1997**, *55*, 8143–8147.
(41) Hyde, B. G.; Andersson, S.; Bakker, M.; Plug, C. M.; O'Keeffe, M. *Prog. Solid State Ch.* **1979**, *12*, 273–327.
(42) Bi, X. X.; Ganguly, B.; Huffman, G. P.; Huggins, F. E.; Endo, M.; Eklund, P. C. *J. Mater. Res.* **1993**, *8*, 1666–1674.
(43) Teschner, D.; Révay, Z.; Borsodi, J.; Hävecker, M.; Knop-Gericke, A.; Schlögl, R.; Milroy, D.; Jackson, S. D.; Torres, D.; Sautet, P. *Angew. Chem., Int. Ed.* **2008**, *47*, 9274–9278.
(44) Loffreda, D. *Surf. Sci.* **2006**, *600*, 2103–2112.
(45) Reuter, K.; Scheffler, M. *Phys. Rev. Lett.* **2003**, *90*, 046103−1-046103−4.

Scheme 1. Qualitative Interpretation of the ab Initio Atomistic Thermodynamics Study of the Iron Carbide Structures[a]

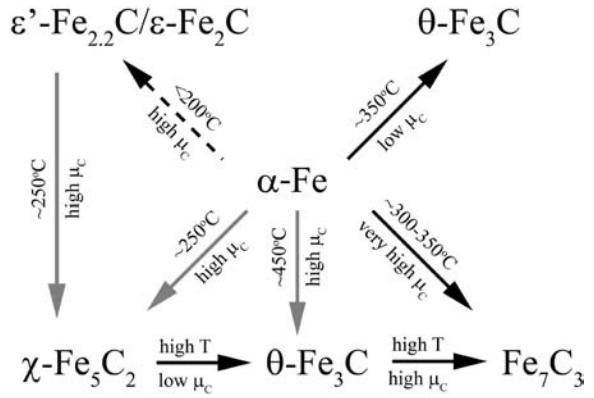

[a] Gray arrows indicate transformations where entropic contributions to the total free energy may be significant. The dashed arrow indicates that the transformation might be kinetically inhibited.

First of all, the model reactions $CO + H_2 \rightarrow C + H_2O$ and $2\,CO \rightarrow C + CO_2$ are a necessary, but unrealistic, simplification during FTS conditions. At the surface, there is competition for carbon atoms for bulk carbide formation, reaction into hydrocarbons, and the Boudouard reaction forming graphitic surface carbon. This is not taken into account in our model. Additionally, the reactants and products might not behave as ideal gases during FTS at higher pressures. Typically, vapor phase, liquid, and solid (waxes) products are formed under FTS conditions, invalidating the ideal gas behavior assumed in our thermodynamic calculations. Moreover, the typical FTS reactor is not a batch reactor run under gas phase equilibrium conditions. FTS takes place in a continuous flow of reactants and products through and from the reactor. Although we used as reasonable conditions as possible for our calculations, there might be an offset between the partial pressures of gases experienced by the catalyst in the real reactor as compared to our model. Finally, as noted above, the ab initio thermodynamics approach adopted here can only be used to estimate the relative thermodynamic stability of phases in contact with a certain gas mixture at a certain temperature and pressure. Entropic contributions, as well as kinetic and diffusion barriers, which may play an important role in the (trans)formation of the solids, are not calculated.

However, being aware of the limits of the model adopted for the evaluation of μ_C, we will show that, in spite of the offset, the general observed trends can be explained and, as such, the calculations form a useful base in interpreting the experimental results presented in this paper.

As a final remark, it should be noted here that the oxygen chemical potential μ_O also has an influence on the formed phases during FTS. α-Fe or carbide phases can be oxidized during FTS by interaction with H_2O. However, in order to simplify the discussion, we will consider the oxidation of the α-Fe and carbide phases to be a separate process from the carburization of α-Fe and therefore will not include the influence of μ_O.

3.2. Influence of μ_C on the Formed Carbide Phases during Pretreatment. Figure 3 shows the calculated μ_C for different mixtures of CO in H_2 ($pCO < pH_2$) at 1 bar total pressure for the reaction $2\,CO \rightarrow C + CO_2$ and $CO + H_2 \rightarrow C + H_2O$, as well as μ_C for the same reaction under FTS reaction conditions at different pressures and temperatures. From the figure, it follows that μ_C changes from −6.50 eV in the case of pure CO at 350 °C to −6.74 eV in the case of 1% CO in H_2 at 350 °C. In case the adsorbed oxygen atoms produced by CO dissociation would be preferentially removed by H_2, theoretically, the μ_C for the reaction would be even lower. However, since mass spectrometry data (after catalyst reduction) mainly showed CO_2 evolution during our experiments, we exclude this reaction pathway for now. It can be inferred from the calculations that lowering the concentration of CO to 1% at 350 °C has the same effect on μ_C as increasing the temperature of pure CO gas to 450 °C. Therefore, varying the partial pressure of CO poses an attractive way of changing μ_C at constant temperature. As it was found that pretreatment in CO at higher temperatures than 350 °C led to a dramatic increase in deposition of surface carbon on the carbide phases (see Figures S7 and S8 in the Supporting Information), lowering the CO partial pressure could offer an alternative way of synthesizing surface-carbon-free θ-Fe_3C. As discussed in conjunction with the DFT method and reference carbide synthesis in the Supporting Information, because of the difficulty in distinguishing between ϵ-Fe_2C and ϵ′-$Fe_{2.2}C$ using XRD[11,24] and XAFS, we will not further distinguish between these phases below and will generally refer to them as ϵ-carbides.

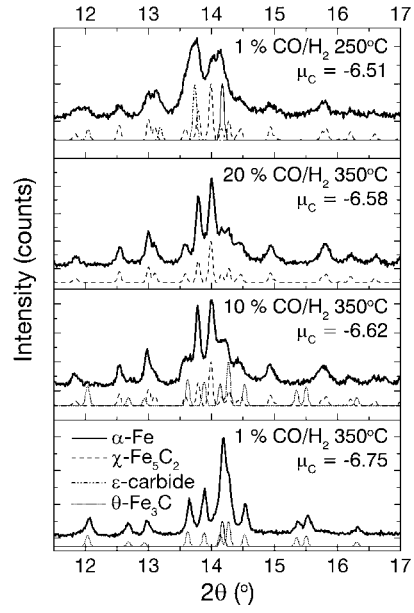

Figure 4. XRD patterns of the α-Fe_2O_3 catalyst material after different pretreatment procedures, imposing different μ_C. The theoretical XRD patterns for the different crystal structures are shown below each experimental pattern.

Figure 4 shows the *ex situ* experimental XRD patterns of α-Fe_2O_3 catalyst samples pretreated at 1%, 10%, and 20% CO in H_2 at 350 °C. Also included is the same sample treated in 1% CO at 250 °C ($\mu_C = 6.51$ eV), after reduction in H_2 at 350 °C. TEM analysis (Figure S9 in the Supporting Information) showed that the initial catalyst consisted of very small (<5 nm) α-Fe_2O_3 crystallites in combination with some larger ∼30 nm crystallites. The catalyst sample had a characteristicly high BET surface area of 136 m^2/g (0.17 mL/g pore volume). After treatment at 350 °C in 1% CO in H_2, the catalyst sample formed a mixture of mainly θ-Fe_3C and residual α-Fe. XRD profile refinement yielded a contribution of 75 vol % θ-Fe_3C and 25 vol % α-Fe with crystallite sizes of ∼26 and ∼21 nm, respectively. The samples treated in 10% CO/H_2 (higher μ_C) formed a mixture of χ-Fe_5C_2, θ-Fe_3C, and ϵ-carbides. The treatment in 20% CO in H_2 formed 94 vol % χ-Fe_5C_2 and 6 vol % ϵ-carbides. At lower temperatures, a higher contribution of the ϵ-carbides was observed: the sample treated in 1% CO in

Table 3. *Ex Situ* XRD Analysis of the Catalyst Materials Pretreated under Different Conditions

Treatment	Calculated gas phase μ_C (eV)	α-Fe (vol %)[a]	θ-Fe_3C (vol %)[a]	ϵ-carbides (vol %)[a]	χ-Fe_5C_2 (vol %)[a]	BET surface area (m^2/g)	Pore volume (mL/g)
1% CO/H_2 350 °C	−6.75	25 (26 nm)	75 (21 nm)	−	−	13	0.07
10% CO/H_2 350 °C	−6.62	−	20 (10 nm)	6 (20 nm)	74 (22 nm)	18	0.15
20% CO/H_2 350 °C	−6.58	−	−	6 (18 nm)	94 (14 nm)	25	0.19
1% CO/H_2 250 °C, after reduction H_2 350 °C	−6.51	10 (22 nm)	−	21 (20 nm)	69 (24 nm)	12	0.04

[a] Parenthetical values indicate XRD crystallite sizes. Errors: vol % ±5%, crystallite sizes ±10%.

H_2 at 250 °C after reduction for 2 h in H_2 at 350 °C formed a mixture of χ-Fe_5C_2, ϵ-carbides, and α-Fe. As discussed above, the ϵ-carbides are stable with respect to the χ-Fe_5C_2 and θ-Fe_3C phase at high μ_C and low temperature (Figure 2). At higher temperatures and lower μ_C, the ϵ-carbides are transformed into χ-Fe_5C_2. It is noted here that the formation of the ϵ-carbides was also observed under similar conditions in an earlier *in situ* FTS study.[5] Table 3 summarizes the quantification of the different phases formed in the samples after their respective treatments.

The results are in agreement with the predicted stability of the different carbide phases as a function of the chemical potential μ_C. Low μ_C leads to the preferential formation of θ-Fe_3C, and high μ_C to the formation of χ-Fe_5C_2. At even higher μ_C conditions and lower temperatures, ϵ-carbides are formed preferentially.

Except for the influence on μ_C, it is observed that the treatment in mixtures of CO/H_2 at lower partial pressures of CO also has an effect on the carburization rates. Both 1% CO/H_2 samples show a remaining contribution of α-Fe after 2 h, indicating that the carburization kinetics are significantly lower at lower partial pressures of CO. Interestingly, the sample pretreated in 1% CO/H_2 at 350 °C does not show any ϵ-carbides or χ-Fe_5C_2. This illustrates the low stability of ϵ-carbides at low μ_C and suggests that the θ-Fe_3C carbide might be formed directly from α-Fe under these conditions, and thus at a lower rate compared to the shear/twinning induced $\alpha-\epsilon-\chi-\theta$ transition.[25,26] Alternatively, under these conditions, the transformation of the ϵ-carbides and χ-Fe_5C_2 to θ-Fe_3C might be too rapid to be observed in *ex situ* XRD.

There was a clear effect of the treatments on the surface texture of the catalyst materials. N_2 physisorption showed that the catalyst materials treated with higher concentrations of CO typically showed somewhat higher BET areas. Accordingly, TEM analysis showed a significantly larger particle size for the catalysts pretreated at lower CO pressures (Figure S9 in the Supporting Information). Table 3 summarizes the surface texture properties of the catalyst after treatment. The surface areas and pore volumes of the materials were higher for 10% and 20% CO treatments. In 1% CO/H_2, the BET surface areas and pore volumes of the materials decreased significantly for the catalysts treated at 250 and 350 °C. Overall, the BET surface areas were lower than that of a sample treated in pure CO at 280 °C (not further discussed here) which was 44 m^2/g with a pore volume of 0.17 mL/g. Typically, as carbides are formed from an oxide precursor, the surface area of the catalyst is observed to increase during carburization, due to shearing and separation of the carbide crystallites from the underlying oxide.[46] Our observations from TEM, XRD, and N_2-physisorption confirm that, in the presence of higher concentrations of H_2, the formed α-Fe phase may sinter before carburization, leading to a collapse of the catalyst pore structure and resulting in the loss of surface area and porosity.

The XRD pattern of the sample prepared at 350 °C in 1% CO in H_2 shows no indication of crystalline carbonaceous deposits. TEM confirmed this observation (Figure SI7 in the Supporting Information). This is very different from the XRD pattern of the θ-Fe_3C reference sample prepared at 450 °C, which showed a significant contribution of (graphitic) carbon (Figures S4b and S7 in the Supporting Information). The lower temperature in combination with the presence of H_2 significantly reduces the laydown of carbon from the Boudouard reaction.

In summary, we have illustrated that by tuning the chemical potential μ_C we have a valuable tool to synthesize specific surface-carbon-free carbide phases, which would otherwise only be formed at high temperature. In the remainder of the paper we will use the chemical potential μ_C to preferentially transform the same parent catalyst material to different relative amounts of the ϵ-carbide, χ-Fe_5C_2, and θ-Fe_3C carbide phases with similar crystallite sizes and without excessive carbonaceous surface deposits. Below, the pretreatment and subsequent high pressure Fischer−Tropsch synthesis will be monitored *in situ* on the long-range order (XRD) and local order scales (EXAFS), while simultaneously measuring carbonaceous surface species by Raman Spectroscopy. This approach will allows us to systematically study the performance of the carbide catalysts as a function of their structure.

3.3. In Situ High Pressure Fischer−Tropsch Synthesis over Catalyst Materials Pretreated at Low μ_C and High μ_C. 3.3.1. Genesis of the Fe-Phases. FTS catalysis, by definition, takes place at the surface of the catalyst. In this research, due to their flexibility for application under high pressure FTS conditions, we apply XRD, XAFS, and Raman spectroscopy for catalyst characterization, which in principle only yield information about the bulk structure of the catalyst. However, we justify the use of bulk techniques to make structure/activity relationships as carbide particle sizes involved in the catalysts are typically very small and the bulk structure of the catalyst indirectly determines the nature of the surface structure of the catalysts.

Figure 5 shows the evolution of the XRD patterns for the catalyst precursor during pretreatment in pure CO to 280 °C

(46) Li, S.; Ding, W.; Meitzner, G. D.; Iglesia, E. *J. Phys. Chem. B* **2001**, *106*, 85–91.

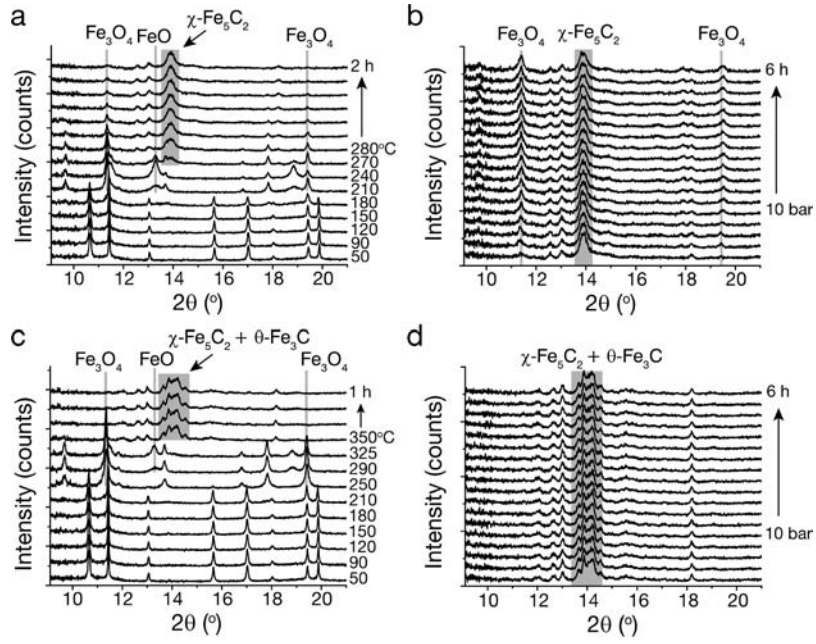

Figure 5. XRD patterns showing the evolution of the crystalline phases in the α-Fe_2O_3 catalyst samples during pretreatment and FTS. (a) During pretreatment in 1 bar of CO at 280 °C (high μ_C) and subsequent FTS (b). (c) During pretreatment in 1% CO in H_2 (low μ_C) at 350 °C and subsequent FTS (d). For clarity, only certain characteristic diffraction lines are indicated in the plots.

and 1% CO in H_2 to 350 °C and the subsequent FTS reaction. For brevity, in the remainder of this paper, the sample pretreated in CO at 280 °C will be referred to as the high μ_C sample, whereas the sample pretreated in 1% CO in H_2 at 350 °C will be referred to as the low μ_C sample.

From the figure it can be inferred that the starting α-Fe_2O_3 phase is converted into Fe_3O_4 and FeO before transforming into the respective carbide phases. No intermediate α-Fe species were found to form, showing that the conversion into the carbide phases was faster in this experiment compared to the *ex situ* experiments. We attribute this difference to the higher gas hourly space velocity applied in the *in situ* experiments and the difference in hydrodynamic flow properties of the capillary reactor compared to the larger quartz tube reactor.[34]

During the treatments, small FeO crystallites were observed. This oxide phase was not observed during the formation of the reference carbides (Figure S4 in the Supporting Information) and most likely stabilized due to the small size of the starting α-Fe_2O_3 crystallites in the catalyst samples.

The XRD data show that, after the respective pretreatments, less crystalline carbide phases are formed compared to the carbide references and *ex situ* experiments. In fact, there are very broad contributions to the XRD patterns of around 14° and 24° 2θ, characteristic for the presence of very small carbide crystallites. Furthermore, the catalysts are not phase pure after their respective pretreatments. The high μ_C catalyst sample mainly consists of χ-Fe_5C_2 but has a contribution of ϵ-carbides (~10 vol %) while the low μ_C catalyst shows a large contribution of χ-Fe_5C_2 (~56 vol %) in addition to θ-Fe_3C (~44 vol %). Apparently, the higher space velocities through the capillary compared to the *ex situ* experiments have a large effect on μ_C, and as a result the phase composition is somewhat different in the *in situ* experiment. We attribute the differences to a lower pCO_2/pCO ratio as a result of the higher space velocities, effectively leading to a higher μ_C. The contribution of the different crystalline phases and particle sizes is given in Table 5.

Table 4. Fe K-Edge EXAFS Fit Results for the Catalyst Materials after Pretreatment

Pretreatment	Absorber-backscatterer	N	$\Delta\sigma^2$ (10^{-3} Å^{-2})	R (Å)	ΔE_0 (eV)
high μ_C	Fe−C	1.2 (2.0)[a]	−0.8	1.91 (1.94)	6.6
	Fe−Fe	7.0 (12.0)[a]	−4.4	2.51 (2.52)	1.8
	Fe−Fe	5.3 (5.0)[a]	−5.2	3.70 (3.57)	−8.2
low μ_C	Fe−C	1.1 (2.0)[b]	−1.0	1.85 (1.89)	11.1
	Fe−Fe	5.2 (11.7)[b]	−2.8	2.51 (2.51)	2.7
	Fe−Fe	7.6 (6.0)[b]	−5.5	3.67 (3.67)	3.9

[a] Parenthetical values represent the χ-Fe_5C_2 carbide reference values. [b] Parenthetical values represent the θ-Fe_3C carbide reference values.

As a result of the lower overall crystallinity and the mixture of carbide phases that is formed, the local coordination of the Fe atoms in the catalyst material, as determined from the Fe K-edge EXAFS spectra before FTS at 250 °C, is also significantly different from that in the χ-Fe_5C_2 and θ-Fe_3C reference carbides. The EXAFS data analysis is summarized in Table 4 and Figure 6. The number of nearest neighbors in the first Fe−C and Fe−Fe shells is about half of that of the references, while the number of neighbors in the second Fe−Fe shell is relatively high. The observed contraction for the first Fe−C and Fe−Fe shells in combination with the relaxation of the second Fe−Fe shell and the slightly negative $\Delta\sigma^2$ values with respect to the reference materials at 250 °C further indicate that there might be a significant contribution of an Fe−Fe shell of higher symmetry, possibly due to the presence of α-Fe or a carbide phase of higher symmetry (e.g., ϵ-carbides). The relative number of C neighbors compared to the first shell Fe neighbors is about the same with respect to the carbide references in both samples, although the ratio is slightly higher in the low μ_C catalyst (0.17 in the θ-Fe_3C and χ-Fe_5C_2 references, vs 0.22 in the catalyst), indicating that a significant fraction of the catalyst might be present as a carbide with a higher C/Fe ratio.

The Fe K-edge XANES spectra of the catalysts after pretreatment (Figure 7) show that the absorption feature at 7111.2 eV is enhanced in the catalyst materials and shows many

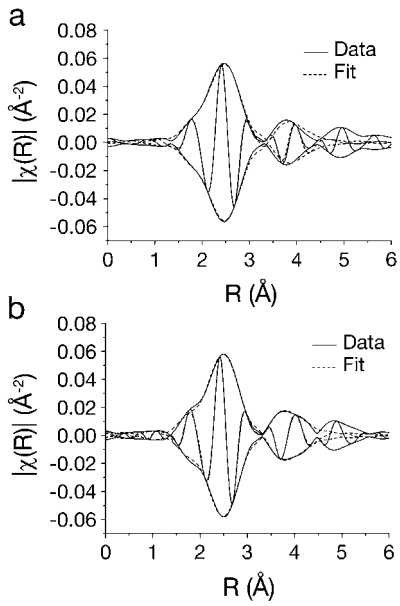

Figure 6. Phase corrected, k^1 weighted Fourier-Transformed Fe K-edge EXAFS data of the α-Fe_2O_3 catalyst samples after pretreatment in CO at 280 °C for 2 h (high μ_C) (a) and after pretreatment in 1% CO/H_2 for 2 h (low μ_C) (b). Solid lines represent the raw data; dashed lines represent the fits.

more similarities to the metallic α-Fe reference than it does to the θ-Fe_3C and χ-Fe_5C_2 references. As a result, linear combination fits (LCF) of the catalyst materials after pretreatment only yielded reasonable fits when including a contribution of the experimental α-Fe spectrum. XRD did not show any additional crystalline phases apart from ϵ-carbides, χ-Fe_5C_2, and θ-Fe_3C; however, EXAFS analysis clearly showed that the contribution of C neighbors in both samples was not significantly lower than that in the reference samples, excluding the presence of pure metallic particles. In fact, the low μ_C sample even showed a somewhat higher contribution of C neighbors compared to the θ-Fe_3C reference. Therefore, we will attribute the contribution of "α-Fe" to the XANES spectrum to an amorphous carbide phase such as Fe_xC, similar to the superparamagnetic carbide phase often reported in Mössbauer studies.[12,24] The exact structure of the carbide is unclear from our results. It is clear that the crystallite sizes involved are too small to refine a carbide structure. However, calculation of XANES spectra using the FEFF code[47] (shown in Figure 7c) showed that the feature at 7111.2 eV is highest for the ϵ-carbides and decreases for χ-Fe_5C_2 and θ-Fe_3C. Furthermore, as the ϵ-carbides were calculated to be thermodynamically stable over the entire carbide stability range (Figure 2), and the contribution of C neighbors is higher than that of the θ and χ carbides, we suggest that the amorphous carbides observed here might be related to ϵ-carbides.

Because of the similarity of the XANES spectra of the θ-Fe_3C and χ-Fe_5C_2 phases, there is a large uncertainty in the contribution of these phases to each spectrum. Therefore, calculated carbide contents will be reported in terms of the total contribution of crystalline θ- and χ-phases and the contribution of amorphous carbide phases. The XANES linear combination fit results are summarized in Table 5. After pretreatment, the low μ_C catalyst contains 49% of the amorphous Fe_xC phase while the high μ_C catalyst contains 24%.

(47) Ankudinov, A. L.; Ravel, B.; Rehr, J. J.; Conradson, S. D. *Phys. Rev. B* **1998**, *58*, 7565–7576.

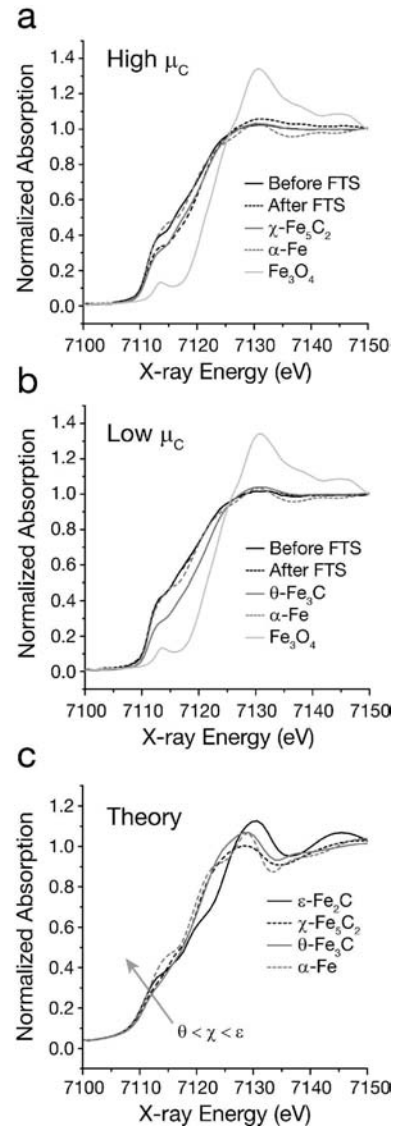

Figure 7. Fe K-edge XANES spectra of the α-Fe_2O_3 catalyst samples after pretreatment and FTS: (a) high μ_C catalyst sample, (b) low μ_C catalyst sample. (c) Calculated XANES spectra using FEFF. The reference compounds are indicated in each subfigure.

Figure 5 shows the evolution of the crystalline phases during the high pressure FTS reaction for the catalyst materials pretreated at low and high μ_C. From the figure, it is clear that the two catalysts behave quite distinctly under FTS conditions.

The catalyst pretreated at high μ_C is gradually oxidized to Fe_3O_4 during FTS. The estimated contribution of Fe_3O_4 in this sample after reaction is 38 vol %, and the crystallite size is about 15 nm. It is not clear whether one specific carbide phase is preferentially oxidized during FTS. However, as the intensity of the χ-Fe_5C_2 peaks in XRD remain almost constant while the Fe_3O_4 peaks increase (and thus the total fraction of crystalline material increases), it is suggested that the amorphous carbide phase in this catalyst is more susceptible to oxidation, forming crystalline Fe_3O_4.

By contrast, the XRD patterns of the catalyst pretreated at low μ_C conditions appears to be quite stable with time-on-stream. Apparently, this catalyst is not readily oxidized to Fe_3O_4. The sample does show a somewhat lower contribution of θ-Fe_3C after FTS and is slowly converted into the thermodynamically more stable χ-Fe_5C_2 phase under the high μ_C FTS conditions.

Table 5. Overview of the Physicochemical and Catalytic Properties of the Catalyst Materials before and after 6 h FTS at 10 bar, 250 °C

Catalyst pretreatment		XAFS[a] (mol %)	XRD[b] (vol %, crystallite size)	Raman	Fischer−Tropsch Performance
High μ_C	Before FTS	χ-Fe_5C_2 (76%), Fe_xC (24%)	χ-Fe_5C_2 (90%, 16 nm) ϵ-carbides (10%, 20 nm)	Some graphitic C	
	After FTS	χ-Fe_5C_2 (74%), Fe_xC (12%), Fe_3O_4 (14%)	χ-Fe_5C_2 (57%, 15 nm) ϵ-carbides (5%, 24 nm) Fe_3O_4 (38%, 15 nm)	No significant increase of graphitic C	Conversion relatively high and increasing with time-on-stream, C_{4+} selectivity high, WGS active
Low μ_C	Before FTS	χ-Fe_5C_2 + θ-Fe_3C (51%), Fe_xC (49%)	χ-Fe_5C_2 (56%, 18 nm) θ-Fe_3C (44% 15 nm)	Some graphitic C	
	After FTS	χ-Fe_5C_2 + θ-Fe_3C (50%), Fe_xC (50%)	χ-Fe_5C_2 (61%, 11 nm) θ-Fe_3C (39%, 13 nm)	Incremental formation of graphitic C	Conversion relatively low, C_{4+} Selectivity decreasing with time-on-stream, pCO_2 low

[a] Errors: ±5 mol %. [b] Errors: ±5 vol %, crystallite sizes ±10%.

In addition, there is a small decrease in the crystallite sizes of the χ-Fe_5C_2 and θ-Fe_3C phases observed.

The diffraction lines at higher angles, around 23°−27° 2θ, due to the (401), (133), (332), and (430) reflections corresponding to a 1.25−1.07 Å *d*-spacing are less pronounced relative to the lower 2θ angles in the samples after 6 h of FTS at 10 bar, especially for the low μ_C catalyst (Figure S10 in the Supporting Information). Because of the angular dependence of the Debye−Waller factor, which is a measure for the thermal, static, and dynamic disorder of crystal structures, this indicates an increase in total disorder after 6 h of FTS at 10 bar. Since the temperature was kept constant during this time, the temperature factor must have increased due to an increase in the static or dynamic disorder of the carbide structures, which suggests the slow transformation of iron carbides into more disordered structures under FTS conditions. Table 5 summarizes the XRD analysis of the catalyst samples after 6 h of FTS at 10 bar.

Table 5 shows the results of the linear combination fitting of the XANES spectra (Figure 7) for both catalysts after 6 h of FTS. A phase composition of 14 (± 5) mol % Fe_3O_4, 74 (± 5) mol % χ-Fe_5C_2, and 12 (± 5) mol % Fe_xC was found for the high μ_C catalyst after FTS. As the Fe atom concentrations per volume are similar for χ-Fe_5C_2 and Fe_3O_4, but might be somewhat higher for Fe_xC, this translates to an estimated volume fraction of 15−25%. This is about half the volume fraction that was estimated by the XRD analysis and emphasizes that especially the contribution of the amorphous carbide phases is underestimated in the XRD analysis. The composition of the low μ_C catalyst, as derived from the Fe K-edge XANES data, remained nearly constant during FTS.

The radial distribution functions during FTS (presented in Figure 8), as derived from the Fe K-edge EXAFS data, confirm the apparent stability of the phases in the catalyst pretreated at low μ_C observed from XRD. There are only very subtle changes in the local structure of this catalyst during the FTS reaction. In contrast, the radial distribution function of the high μ_C catalyst shows dramatic changes with a longer time-on-stream. The first coordination shell grows significantly during the FTS reaction, mainly due to the increasing contribution of Fe−O scattering by oxidation of the carbide phases. In fact, initially, the oxidation of the catalysts shows up more dramatically on the local scale than the changes in long-range structure, as probed by XRD. This might be a further indication for the preferential oxidation of the amorphous Fe_xC phase in this catalyst.

3.3.2. Surface Carbonaceous Species. Figure 9 presents Raman spectra taken from the two catalysts during high pressure

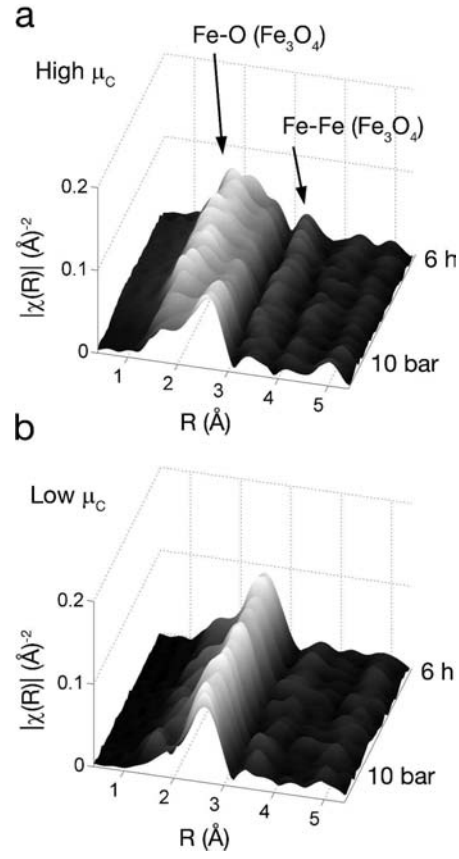

Figure 8. Phase corrected, k^1 weighted Fourier-transformed Fe K-edge EXAFS data of the α-Fe_2O_3 catalyst samples during FTS. (a) High μ_C catalyst and (b) low μ_C catalyst. The arrows indicate the position of the Fe−O and Fe−Fe coordination shells in Fe_3O_4.

FTS. For both catalysts, the Raman spectra show a significant increase in peaks in the region between 1300 and 1600 cm^{-1} with time-on-stream. This spectral region is commonly assigned to the C=C stretching of polyaromatic rings and conjugated olefins.[48] More specifically, the G- (1595 cm^{-1}) and D-bands (1329 cm^{-1})[49] are observed in this region for both materials during the initial FTS. The G-band is assigned to more graphitic-like carbon, while the D-band is only present for more

(48) Chua, Y. T.; Stair, P. C. *J. Catal.* **2003**, *213*, 39–46.
(49) Katagiri, G.; Ishida, H.; Ishitani, A. *Carbon* **1988**, *26*, 565–571.

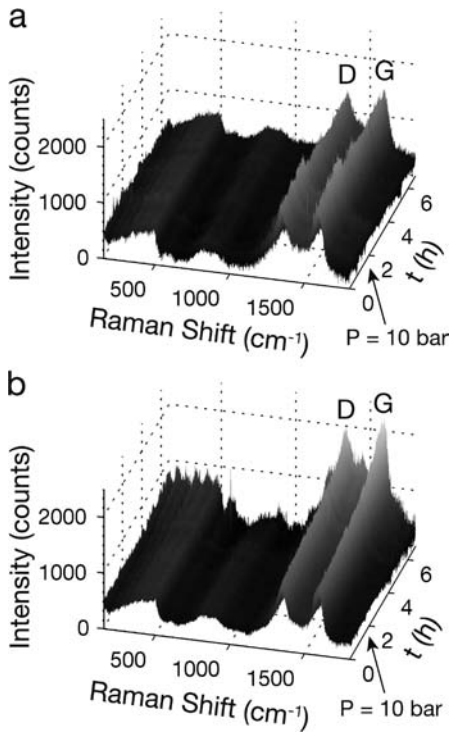

Figure 9. Raman spectra of the (a) high μ_C catalyst and (b) low μ_C catalyst during FTS. The D and G bands are indicated in the figure. The broad peaks at ~500 and 800 cm^{-1} are due to the contribution of the quartz capillary and SiO_2 diluent to the spectra.

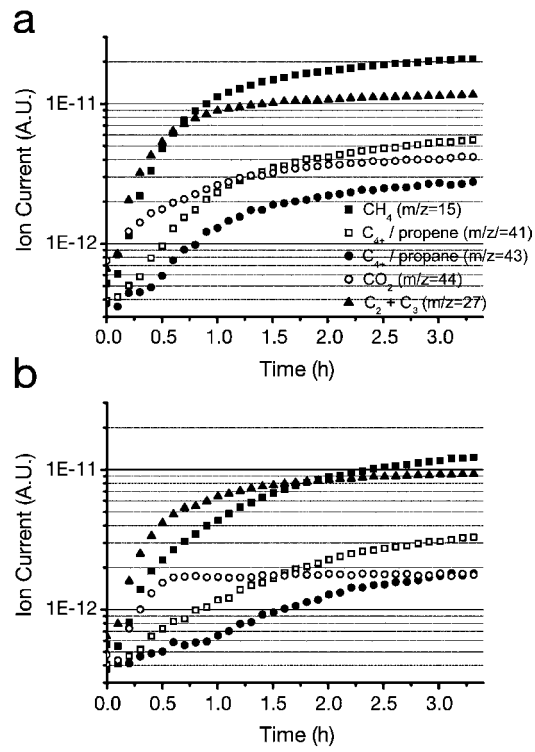

Figure 10. Mass spectrometry data during the first hours of high pressure FTS. (a) High μ_C catalyst and (b) low μ_C catalyst. The data are normalized per g of Fe.

disordered type graphitic carbonaceous species. With time-on-stream, the evolution of the G-band and D-band carbon is dramatically different for the two catalysts. While the D- and G-bands initially increase for the high μ_C catalyst, upon reaching the reaction pressure of 10 bar the intensity of the Raman peaks levels off and is stable with a longer time-on-stream. In sharp contrast, the catalyst pretreated at low μ_C conditions shows a gradual increase in carbon species with a longer time-on-stream. In addition, the ratio of the G-band to the D-band appears to be somewhat higher in the case of the low μ_C catalyst, further evidencing the possible formation of carbon in a two-dimensional sheet-like topology.[48] The formation of graphitic carbon is generally considered to be responsible for catalyst deactivation, as the graphitic overlayers formed might block active sites and the high hydrogenation temperature of graphitic carbon makes the phase very stable during FTS.[50−52]

As we will illustrate, the formed carbonaceous deposits have important implications for the catalytic activity and stability.

3.3.3. Structure−Activity Correlation. The catalytic data, as measured during the *in situ* experiment by online mass spectrometry is presented in Figure 10. For the discussion of the data, we assume that the *m*/*z* peak at 27 is mainly due to short hydrocarbon chain species (ethane/ethane and propane/propene). For longer hydrocarbon chains, this peak is also present, but at lower relative intensities compared to the *m*/*z* 41 and 43 peaks. Propane has a much higher relative intensity of the *m*/*z* 43 peak, while for propene this peak is absent. Hydrocarbon chains of longer than four carbon atoms all show the 41 and 43 mass fragments. CO_2 was characterized by the mass fragment at *m*/*z* 44. Other masses were measured (CO, H_2, He, H_2O) but not reported here for the sake of brevity.

The results shows that the catalyst pretreated at 1% CO/H_2 at 350 °C (low μ_C conditions) forms lower concentrations of C_{4+} hydrocarbons and CO_2. Moreover, for this catalyst the ratio of CH_4 to C_2 and C_3 hydrocarbons appears to be continuously increasing with time-on-stream. The high μ_C catalyst, on the other hand, shows a more stable activity and selectivity with time-on-stream and is more selective to C_{4+} hydrocarbon chains. Below, we will discuss the implications of the catalyst structure on the performance of the catalyst in the high pressure FTS.

Table 5 summarizes the observations from the XAFS/XRD/Raman techniques and the catalytic performance of the catalysts during high pressure FTS. The catalyst pretreated at high μ_C consisted of small χ-Fe_5C_2 crystallites before the FTS reaction. Some crystalline ϵ-carbides were also present. EXAFS/XANES further showed that there was a significant contribution of amorphous Fe_xC carbide crystallites formed during the pretreatment. During FTS, the sample was partly converted into Fe_3O_4. Although Fe_3O_4 is not an active phase in FTS, the catalytic performance data of the catalyst in terms of activity, selectivity, and stability are superior to those of the catalyst pretreated at low μ_C conditions. Fe_3O_4 is an active phase in the water−gas shift reaction, and the higher concentrations of CO_2 measured in this sample indicate that the catalyst is active in the WGS. As a result of this higher WGS activity, the observed increase in catalytic activity with time-on-stream could be partially attributed to the higher partial H_2 pressures as a result of the WGS reaction. In this way, the high WGS activity might also limit the buildup of inactive carbon on the surface of the catalyst as was observed from Raman spectroscopy: Carbonaceous surface species might also be hydrogenated more readily, preventing the buildup of graphitic-like carbon. The high extent

(50) Loaiza-Gil, A.; Fontal, B.; Rueda, F.; Mendialdua, J.; Casanova, R. *Appl. Catal. A: General* **1999**, *177*, 193–203.
(51) Eliason, S. A.; Bartholomew, C. H. *Appl. Catal. A: General* **1999**, *186*, 229–243.
(52) Xu, J.; Bartholomew, C. H. *J. Phys. Chem. B* **2004**, *109*, 2392–2403.

of oxidation in this catalyst is likely to be related to the expected relatively high surface area and pore volume of this catalyst compared to the low μ_C catalyst. Although the exact surface area and porosity of the catalyst could not be determined *in situ*, it has been shown (Table 3) that high concentrations of H_2 during pretreatment led to a loss of surface area and porosity. The buildup of H_2O pressure in FTS catalyst pores is often thought to be the main reason for catalyst oxidation, leading to the formation of a core−shell oxide−carbide structure.[53]

The catalyst pretreated at low μ_C consisted of small θ-Fe_3C and χ-Fe_5C_2 crystallites, in combination with a significant fraction of amorphous Fe_xC. XANES analysis yielded that, before FTS, ∼50% of the Fe in this catalyst was present as the amorphous Fe_xC phase, compared to 24% in the catalyst pretreated at high μ_C. The catalyst showed lower overall activity and lower selectivity to long chain hydrocarbon species compared to the high μ_C catalyst. In addition, this catalyst was found to be much more susceptible to the buildup of ordered surface carbon species during FTS. This buildup is likely to be the cause for the higher observed methane selectivity in this catalyst. Pure Fe^0 is known to be susceptible to the buildup of surface carbon species,[54] and it has been reported that the θ-Fe_3C phase is of a metallic nature[55] and the most stable surface (001)[56] has CO adsorption energies higher than that for Fe (100) and (110).[57] Therefore, the presence θ-Fe_3C might contribute to the buildup of carbonaceous deposits. The overall high metallic nature of this catalyst, as indicated by the high intensity of the 7111.2 eV feature in the XANES spectra (attributed to the ϵ-carbide related, amorphous Fe_xC species), might contribute to the excessive formation of carbonaceous deposits. As the content of amorphous Fe_xC species in the catalyst pretreated at high μ_C was initially significantly lower and decreased with time-on-stream due to oxidation, this might further explain the lower amount of carbonaceous deposits in this catalyst after FTS. The catalyst pretreated at low μ_C conditions was not oxidized under high pressure FTS conditions, and very few changes were observed in the long-range or local structure of the Fe phases. The lower porosity of the catalyst might play a role in the lower extent of oxidation that was observed. The structure of this catalyst became more disordered with time-on-stream, reflected by the diminished intensity of the high 2θ angle θ-Fe_3C peaks in the XRD pattern. This observation indicates the slow transformation of carbide phases during high pressure FTS.

4. Conclusions

The carbon chemical potential μ_C, as imposed by the gas phase conditions, combined with kinetic and entropic effects, can be used to qualitatively explain the transformation of α-Fe into $\epsilon-\chi-\theta$ carbide phases during the pretreatment of iron oxide catalysts and the high pressure FTS reaction. Although ϵ-carbides are enthalpically most stable during typical FTS conditions, kinetic and entropic factors may inhibit their formation in large amounts. χ-Fe_5C_2 is found to have the lowest theoretical deformation energy with respect to the hcp lattice and therefore might be preferentially formed during FTS. Further transformation of χ-Fe_5C_2 into θ-Fe_3C is driven by a higher thermodynamic stability under specific, low μ_C gas phase conditions.

The predicted influence of μ_C on the formed iron carbide phases during pretreatment was illustrated applying pretreatment conditions constituting different μ_C. High μ_C conditions at low temperatures lead to the preferential formation of ϵ-carbides, while low μ_C conditions lead to the formation of θ-Fe_3C. It is found that, under specific low μ_C conditions, θ-Fe_3C might form directly from α-Fe without the presence of excessive amounts of surface carbon.

By pretreating a catalyst material at two extremes of experimentally achievable μ_C conditions, catalysts of different carbide compositions were synthesized and characterized during the high pressure FTS reaction. Due to the small crystallite sizes of the initial α-Fe_2O_3 phase in the catalyst samples, amorphous Fe_xC crystallites (with a structure similar to ϵ-carbides) are formed and FeO is observed as an intermediate phase during catalyst reduction.

The catalyst formed after pretreatment in pure CO at 280 °C (high μ_C conditions) contains mainly χ-Fe_5C_2 and is more active and selective in the FTS reaction, but susceptible to oxidation. The oxidation of the catalyst is more pronounced on the local coordination scale (EXAFS) compared to the long-range crystalline order (XRD), indicating the possible preferential oxidation of amorphous carbide phases. The porous nature of the catalyst material, induced by the high carburization rates at low temperatures (∼280 °C), is likely to contribute to the high extent of oxidation.

The catalyst pretreated in 1% CO/H_2 at 350 °C (low μ_C conditions) contains ∼50% crystalline θ-Fe_3C, ∼50% χ-Fe_5C_2, and a high fraction of amorphous Fe_xC. The catalyst is much more susceptible to the buildup of surface graphitic carbonaceous deposits during FTS. The lower porosity of the catalyst, induced by the carburization at higher temperatures (∼350 °C), leads to a lower susceptibility to oxidation, while the more metallic nature of the θ-Fe_3C and Fe_xC phases is likely to contribute to the higher formation rate of inactive carbonaceous surface species. A slow transformation of θ-Fe_3C to χ-Fe_5C_2 is observed under high pressure FTS conditions.

More generally, our results illustrate how μ_C can be used as a descriptor for thermodynamically induced phase changes in catalyst (and other solid state) systems. Fe-based FTS catalysts were characterized at high pressure FTS conditions for the first time, and it was found that amorphous phases can play a significant role in Fe-based FTS catalysts. Therefore, XAFS/XRD proved to be a valuable combination of techniques, allowing the characterization of amorphous and crystalline phases at realistic reaction conditions, while Raman spectroscopy could be applied at the same conditions to study surface carbon species. Finally, our findings illustrate how the synergy of theoretical and experimental methods can be applied to obtain valuable insights into complex catalyst systems.

Acknowledgment. B.M.W. acknowledges funding from Shell Global Solutions and the Dutch Science Foundation (NWO/CW). Dr. W. Bras of the Dutch Belgian (DUBBLE) beamlines at the

(53) Dry, M. E., In *Catalysis - Science and Technology*, Anderson, J. R.; Boudart, M., Eds. Springer-Verlag: New York, 1981; Vol. 1, pp 160−255.
(54) Dwyer, D. J.; Hardenbergh, J. H. *J. Catal.* **1984**, *87*, 66–76.
(55) Häglund, J.; Grimvall, G.; Jarlborg, T. *Phys. Rev. B* **1991**, *44*, 2914–2919.
(56) Chiou Jr., W. C.; Carter, E. A. *Surf. Sci.* **2003**, *530*, 87–100.
(57) Liao, X.-Y.; Cao, D.-B.; Wang, S.-G.; Ma, Z.-Y.; Li, Y.-W.; Wang, J.; Jiao, H. *J. Mol. Catal. A-Chem* **2007**, *269*, 169–178.
(58) Yakel, H. L. *Int. Mater. Rev.* **1985**, *30*, 17–44.
(59) Fruchart, D.; Chaudouet, P.; Fruchart, R.; Rouault, A.; Senateur, J. P. *J. Solid State Chem.* **1984**, *51*, 246–252.
(60) Hofer, L. J. E.; Cohn, E. M.; Peebles, W. C. *J. Am. Chem. Soc.* **1949**, *71*, 189–195.
(61) Retief, J. J. *Powder Diffr.* **1999**, *14*, 130–132.
(62) Herbstein, F. H.; Snyman, J. A. *Inorg. Chem.* **1964**, *3*, 894–896.
(63) Hirotsu, Y.; Nagakura, S. *Acta Metall.* **1972**, *20*, 645–655.

European Synchrotron Radiation Facility (ESRF), Grenoble is acknowledged for arranging access to the experimental facilities at the Swiss-Norwegian beamlines through the SNBL/DUBBLE collaboration agreement. We further acknowledge the ESRF for provision of synchrotron radiation facilities, and we thank Dr. H. Emerich for assistance in using the beamline. We wish to thank Mr. C. van der Spek for TEM analysis and Mr. A. J. M. Mens for N_2-physisorption measurements. Dr. M. G. O'Brien and Dr. S. T. Korhonen are acknowledged for their help in the XAFS/XRD/Raman data acquisition. We thank the Pôle Scientifique de Modélisation Numérique (PSMN) (Lyon) and Dr. F. M. F. de Groot (UU) for the allocation of CPU time.

Supporting Information Available: Complete ref 31, detailed procedures for thermodynamic/DFT calculations, description of the *in situ* high pressure combined XAFS/XRD/Raman setup, XAFS/XRD data analysis procedures and XANES calculations, χ-Fe_5C_2 and θ-Fe_3C reference compound synthesis and *in situ* characterization, TEM images of catalysts pretreated at different μ_C conditions, and full 2θ range XRD patterns of the high/low μ_C catalysts before and after FTS. This material is available free of charge via the Internet at http://pubs.acs.org.

JA105853Q